

Ellipsoidal Variability in the OGLE Planetary Transit Candidates

E. Sirko & B. Paczyński

Princeton University Observatory, Princeton, NJ 08544-1001, USA

E-mail: esirko@astro.princeton.edu

E-mail: bp@astro.princeton.edu

ABSTRACT

We analyze the photometry of 121 OGLE stars with periodic transit events for the presence of ellipsoidal light variations, which indicate the presence of massive companions. We find that over 50% of objects may have stellar companions, mostly among the short period systems. In our Table 1 stars with no measurable ellipsoidal variability are marked as the prime candidates for planetary searches. There is a prospect of improving the analysis, and the systems with smaller ellipsoidal variability will be identified, when the correlations in the OGLE photometry are corrected for in the future, thereby providing a cleaner list of systems with possible planets.

Subject headings: planetary systems – surveys – techniques: photometric

1. Introduction

The first extra solar planet discovered to exhibit photometric transits was HD 209458 (Charbonneau et al. 2000, Henry et al. 2000), but its orbit had been first determined spectroscopically (Mazeh et al. 2000). Massive efforts to detect photometric transits on their own put at least 23 teams into the competition (Horne 2003). By far the largest list of periodic transit candidates was published by the OGLE team (Udalski et al. 2002a,b,c), with a total of 121 objects, with all photometric data available on the Web. The first confirmation that at least one of these has a ‘hot Jupiter’ planet was obtained by Konacki et al. (2003). They also found that a large fraction of OGLE candidates were ordinary eclipsing binaries blended with a brighter star which was not variable, and its light diluted the depth of the eclipses, so they appeared as shallow transits.

It was clear from the beginning that many transits may be due to red dwarfs or brown dwarfs, and that some of these massive companions may give rise to ellipsoidal light variability (Udalski et al. 2002a). In fact in that paper OGLE-TR-5 and OGLE-TR-16 were

noted to exhibit such a variability, indicating that the companion mass had to be substantial. Ellipsoidal variability is a well known phenomenon among binary stars (cf. Shobbrook et al. 1969, and references therein). Tidal effects are responsible for making a star elongated toward the companion. Ellipsoidal variability is due to the changes in the angular size of the distorted star and to gravity darkening, with half of the orbital period. Obviously, the more massive the companion, and the closer it is to the primary, the stronger the effect. It can be used to remove from the OGLE sample objects which have massive, and therefore not planetary, companions (Drake 2003).

The aim of this paper is to extend the work of Drake (2003) to the new list of OGLE transit candidates (Udalski 2002c) and to provide a more realistic error analysis, which is needed in order to assess the reality of ellipsoidal variability.

2. Data Analysis

We took all photometric data from the OGLE Web site:

[http://sirius.astrouw.edu.pl/~ ogle/](http://sirius.astrouw.edu.pl/~ogle/)

[http://bulge.princeton.edu/~ ogle/](http://bulge.princeton.edu/~ogle/)

There are three data sets: two provide a total of 59 objects in the field close to the galactic center (Udalski et al. 2002a,b), and the third provides 62 objects in a field in the Galactic Disk in Carina (Udalski et al. 2002c). There are typically 800 data points for OGLE-TR-1 - OGLE-TR-59, and 1,150 data points for OGLE-TR-60 - OGLE-TR-121. The Carina data set had somewhat longer exposures and the field was much less crowded, so the photometric accuracy is somewhat better than in the Galactic Center field.

To analyze the light curves for ellipsoidal variability the data points within the transits must first be removed. Our algorithm was to start at mid-transit, working outwards, and to reject data points until the third data point whose error placed it within or brighter than the baseline magnitude. We then obtained a five parameter fit to the rest of the data:

$$I_k = \langle I \rangle + a_{c1} \cos p_k + a_{s1} \sin p_k + a_{c2} \cos 2p_k + a_{s2} \sin 2p_k, \quad (1)$$

where I_k is data point number k , and p_k is its phase calculated with the orbital period provided by Udalski et al. (2002a,b,c). The phase is $p = 0$ at mid transit. The values of all five parameters: $\langle I \rangle$, a_{c1} , a_{s1} , a_{c2} , and a_{s2} were calculated with a least squares method. The formal errors for all the sinusoidal coefficients for a given star were practically the same.

In the five parameter fit given with eq. (1) the term a_{c2} corresponds to the ellipsoidal light variations. Tidal effects make a star the brightest at phases 0.25 and 0.75, and the

dimmest at phases 0.0 and 0.5. This corresponds to $a_{c2} > 0$, as the I magnitude is largest when the star is at its dimmest. The values of a_{c2} with their nominal error bars are shown in Fig. 1. Note that for a number of stars the coefficient is negative, many standard deviations smaller than zero. This clearly shows that the nominal errors are not realistic. This is understandable, as there are strong correlations between the errors of consecutive photometric data points (Kruszewski & Semeniuk 2003).

The rms deviation between the five parameter fit and the data is a measure of the photometric errors for individual measurements. The rms errors and the average of the formal errors of the four sinusoidal coefficients of the fit are shown in Fig. 2 with black circles and green triangles, respectively. The formal errors for the fitted parameters are approximately $N^{1/2}$ times smaller than the rms values, as expected; N is the number of photometric data points for a given star. Open symbols refer to the stars in the Galactic Center field, and filled symbols to the stars in Carina. The red squares will be explained later.

It is clear that the errors increase with the I magnitude, as expected. The errors are smaller for the Carina stars, as expected. Two stars, OGLE-TR-24 and OGLE-TR-58, show anomalously large rms. Inspection of their light curves shows they exhibit long term changes of about 0.015 magnitudes. The nature of this variability is not known, and we exclude these two objects from the error histogram shown in Fig. 4, discussed below. The orbital periods are not known for OGLE transits #43, #44, #45, and #46, so these stars are not considered in this paper. The following analysis was done for the remaining 117 objects.

The planetary transit candidates have orbital periods in the range 0.57 – 9.2 days, which corresponds to the frequency of ellipsoidal variability in the range 0.22 – 3.5 d⁻¹. We calculated power spectra for every star as follows:

$$p_\nu = a_{c,\nu}^2 + a_{s,\nu}^2, \quad \nu = \frac{i}{250 \text{ day}}, \quad i = 1, 2, 3, \dots, 1000, \quad (2)$$

where

$$a_{c,\nu} = \frac{\sum_{k=1}^N I_k \cos(2\pi\nu t_k)}{\sum_{k=1}^N \cos^2(2\pi\nu t_k)}, \quad a_{s,\nu} = \frac{\sum_{k=1}^N I_k \sin(2\pi\nu t_k)}{\sum_{k=1}^N \sin^2(2\pi\nu t_k)}, \quad (3)$$

where the summation is done over all photometric data points for a given star, excluding the data points within the transits.

An example of the power spectrum is shown in Fig. 3 for OGLE-TR-5. Also shown is a power law fit to the spectrum:

$$p_{\nu,f} = p_0 \nu^{p_1}, \quad (4)$$

where the two parameters p_0 and p_1 were calculated for each star using a least squares method. The binary period for OGLE-TR-5 is given by Udalski et al. (2002a) as 0.8082

days. The arrows correspond to the orbital frequency $1/P_{\text{orb}} = 1.237 \text{ d}^{-1}$, and the expected frequency of ellipsoidal variability $2/P_{\text{orb}} = 2.475 \text{ d}^{-1}$.

We calculated power spectra for all stars, and each was fitted with its own power law. For every star and for every frequency we calculated the coefficients $a_{c,\nu}$ and $a_{s,\nu}$, as defined by eq. (3), and divided each by $b_\nu \equiv (p_{\nu,f}/2)^{1/2}$ to normalize it. A histogram of these normalized terms is shown in Fig. 4. Also shown is Gaussian distribution with unit variance; it is fairly similar to the histogram, which implies that b_ν provides a reasonable estimate of the statistical error.

For every star we calculated the a_{c1} and a_{c2} terms of eq. (1) and estimated their errors b_1 and b_2 as b_ν evaluated at the corresponding frequencies. The errors for the a_{c2} term, b_2 , are shown in Fig. 2 as red squares. It is clear that these statistical errors are much larger than the errors shown as green triangles, which were based on the assumption that all photometric data points are uncorrelated. The ‘green triangle’ error bars were used in our Fig. 1, which provided the first hint that they are underestimates of the true errors, as so many values of the ellipsoidal variability parameter a_{c2} were negative with very small ‘green’ error bars.

The two amplitudes a_{c2} and a_{c1} are shown in Fig. 5 and Fig. 6, respectively, as a function of orbital period. Negative values of a_{c2} are physically meaningless, and presumably these are $a_{c2} \approx 0$ which were ‘scattered’ to negative values by statistical errors. Indeed, there are 29 negative values, with 20 within one σ of zero, and 9 outside of one σ , with the ratio 20/9 close to that expected for a Gaussian distribution. This also implies that our error estimate is realistic; here and in the following we take $\sigma = b_1$ for a_{c1} and a_{s1} , $\sigma = b_2$ for a_{c2} and a_{s2} .

We expect that about the same number, 29, of positive a_{c2} values is due to errors, while the remaining $117 - 29 - 29 = 59$ are real ellipsoidal variables. This estimate suggests that $\sim 50\%$ of all OGLE transit candidates have massive companions, not planets. Tidal effects responsible for ellipsoidal variations increase strongly with reduced orbit size, and therefore they are expected to be more common at short orbital periods. Indeed, this appears to be the case in Fig. 5.

Ellipsoidal variability scales with the mass ratio, and for low mass companions like planets it becomes much smaller than our errors. Hence, all OGLE transit stars with measurable ellipsoidal variability should be excluded from the list of planetary candidates. Note that blending with non-variable stars dilutes the variable component, and may suppress the amplitude of the apparent ellipsoidal variability.

Some stars vary with the orbital period. Positive values of a_{c1} , as shown in Fig. 6, may indicate a heating (reflection) effect of the companion by the primary, as in the well known

case of Algol, or they may indicate that the true orbital period is twice longer than listed by OGLE, and the variability is ellipsoidal. In the former case nothing can be said about the companion mass; in the latter case the companion is too massive to be a planet.

Note that there are 44 stars in Fig. 6 with negative values of a_{c1} , and 27 of these are within their 1σ error bars of zero. This is consistent with no credible negative a_{c1} . As the errors are expected to be symmetric there must be ~ 40 stars which nominally have positive values of a_{c1} , but in fact are consistent with $a_{c1} = 0$. Unfortunately, we cannot point the remaining 37 stars which may have real ‘reflection’ effects, except for OGLE-TR-39, which has the orbital period given as 0.8 days, and it obviously has $a_{c1} > 0$. This star shows large values (in terms of their errors) of both terms: a_{c1} and a_{c2} . This indicates that the orbital period is correct, the companion has its hemisphere facing the primary noticeably heated, and its mass is large enough to induce ellipsoidal light variations. The reflection effect is expected to be stronger for binaries with small separations, i.e. short orbital period. There is some evidence for this effect in Fig. 6.

Table 1 lists all OGLE transit candidates with known orbital periods, giving their OGLE-TR number, average magnitude $\langle I \rangle$, orbital period P_{orb} in days, and the a_{c1} and a_{c2} coefficients with their errors in milli-magnitudes. In this list of 117 stars 52 are marked with a *, to indicate that their ellipsoidal variability is close to zero, i.e. either negative or within one σ of zero. These are good candidates to have planetary companions. Of course, the selection is statistical: some stars marked with * may have non-zero ellipsoidal variability, and some stars which are not marked may turn out not to exhibit ellipsoidal variability. Still, the list as marked should be ‘cleaner,’ and it should be the primary target for spectroscopic follow-up observations. The total number of non-planetary systems may be larger, and it may become possible to recognize their ellipsoidal light variations if the systematic errors are reduced by a more thorough analysis carried out by Kruszcwski & Semeniuk (2003).

It is interesting to plot a_{c1} versus a_{c2} , as shown in Fig. 7. It is clear that while there are several possibly real positive a_{c1} terms, there are considerably more positive a_{c2} terms.

In a simple model where the presence of a companion may give rise to ellipsoidal light variations and the ‘reflection’ effect the terms a_{s1} and a_{s2} in eq. (1) should be zero. Fig. 8 presents these coefficients in units of their errors. There are 29 stars with a_{s2} having absolute value larger than one σ , with 88 values smaller than one σ . The corresponding numbers for a_{s1} are 41 and 76, respectively. This is close to the ratio expected if the true values of both coefficients were zero, and their errors were Gaussian. The average and the rms values are: $\langle a_{s1}/b_1 \rangle = -0.27$, $\langle a_{s2}/b_2 \rangle = +0.10$, $\langle (a_{s1}/b_1)^2 \rangle^{1/2} = 1.17$, and $\langle (a_{s2}/b_2)^2 \rangle^{1/2} = 0.93$. All this implies that our error estimate is reasonable. Note that

OGLE-TR-68, with $a_{s1}/b_1 = -4.4$, may have a real variability, possibly induced by a spot on the star.

3. Discussion

It is interesting to compare our errors, given in Table 1, with those estimated by Drake (2003). Our errors are also shown in Fig. 2 as red squares, while Drake’s errors are approximately those shown with green triangles. For the faintest stars, for which the systematic errors are comparable to the photon noise, there is only a small difference, approximately a factor of 2. For the bright stars photon noise is negligible compared to systematic errors, and our estimate is ~ 5 times larger than Drake’s. We stress that our estimate is realistic, as demonstrated with Fig. 7 and Fig. 8, while Drake underestimated the errors by a factor of several, as he did not notice strong correlations in the photometric errors. A good example is OGLE-TR-5, with its spectrum shown in Fig. 3. The peak corresponding to the ellipsoidal variability at $2/P_{\text{orb}} = 2.48 \text{ d}^{-1}$ is strong and certainly real. The amplitude is $a_{c2} = 7.5 \text{ mmag}$ in our Table 1, and 7.2 mmag in Drake’s Table 1. However, the errors are 1.3 mmag and 0.4 mmag , respectively. The power spectrum presented in Fig. 3 clearly shows a high level of noise, which is used for our error estimate.

In the case of OGLE-TR-5 the ellipsoidal variability is highly significant with either of the two error estimates. It is not so with OGLE-TR-40, which is listed by Drake as being ellipsoidal variable at the 3.5σ level, while our analysis puts it at just a one σ level, i.e. nothing definite can be said about this case.

The star with the first planetary companion confirmed spectroscopically, OGLE-TR-56 (Konacki et al. 2003), should not have a measurable value of a_{c2} , and reassuringly we do not detect a significant ellipsoidal variability (cf. Table 1). The planetary disk covers $\sim 2 \times 10^{-4}$ of the sky as seen from the star, i.e. the reflection effect has to be small, $a_{c1} < 0.1 \text{ mmag}$. The measured value is $a_{c1} = 1.08 \pm 0.46 \text{ mmag}$, and presumably it is not significant.

A thorough analysis of various systematic effects apparent in the photometry of tens of thousands of variable and non-variable stars measured in the OGLE fields is currently being done by Kruszcwski & Semeniuk (2003). Preliminary results indicate that various systematic errors may be reduced considerably. This may allow a detection of smaller ellipsoidal effects than we could find, and may provide a cleaner list of systems which are likely to have planetary companions. At this time spectroscopists may use our Table 1 to select stars for their planetary search, eliminating objects with measurable ellipsoidal variability, as it implies a large mass ratio, and most likely a red dwarf companion.

It is a pleasure to acknowledge many useful suggestions and discussions with A. Kruszewski, R. Lupton, S. Ruciński and A. Udalski. This research was supported by the NASA grant NAG5-12212 and the NSF grant AST-0204908.

REFERENCES

- Charbonneau, D., Brown, T. M., Latham, D. W., & Mayor, M. 2000, *ApJ*, 529, L45
- Drake, A. J. 2003, *astro-ph/0301295*
- Henry, G. W., Marcy, G. W., Butler, R. P., & Vogt, S. S. 2000, *ApJ*, 529, L41
- Horne, K. 2003, *astro-ph/0301250*
- Konacki, M., Torres, G., Jha, S., & Sasselov, D. D. 2003, *Nature*, 421, 507
- Kruszewski, A., & Semeniuk, I. 2003, in preparation
- Mazeh, T., Naef, D., Torres, G., Latham, D. W., Mayor, M. et al. 2000, *ApJ*, 532, L55
- Shobbrook, R. R., Herbison-Evans, D., Johnston, I. D., & Lomb, N. R. 1969, *MNRAS*, 145, 131
- Udalski, A., Paczyński, B., Zebruń, K., Szymański, M., Kubiak, M. et al. 2002, *AcA*, 52, 1
- Udalski, A., Zebruń, K., Szymański, M., Kubiak, M., Soszyński, I. et al. 2002, *AcA*, 52, 115
- Udalski, A., Szewczyk, O., Zebruń, K., Pietrzyński, G., Szymański, M. et al. 2002, *AcA*, 52, 317
- Wilson, Wilson, R. E., & Deviney, E. 1971, *ApJ*, 166, 605

Table 1. List of transits

Object name	$\langle I \rangle$	P_{orb}	a_{c1}	a_{c2}
OGLE-TR-1*	15.655	1.601	1.18 ± 0.92	-0.24 ± 0.86
OGLE-TR-2	14.173	2.813	-1.13 ± 0.83	2.86 ± 0.76
OGLE-TR-3	15.564	1.189	2.60 ± 0.73	2.67 ± 0.67
OGLE-TR-4*	14.714	2.619	0.01 ± 1.24	0.28 ± 1.15
OGLE-TR-5	14.877	0.808	1.30 ± 1.32	7.50 ± 1.28
OGLE-TR-6	15.351	4.549	4.80 ± 1.36	3.00 ± 1.25
OGLE-TR-7	14.795	2.718	0.78 ± 1.18	1.88 ± 1.05
OGLE-TR-8	15.647	2.715	2.50 ± 1.47	2.02 ± 1.32
OGLE-TR-9	14.010	3.269	0.39 ± 0.82	0.77 ± 0.73
OGLE-TR-10	14.928	3.101	-1.02 ± 1.05	1.29 ± 0.93
OGLE-TR-11	16.007	1.615	0.04 ± 0.80	1.65 ± 0.74
OGLE-TR-12*	14.673	5.772	0.16 ± 0.83	-1.39 ± 0.77
OGLE-TR-13	13.893	5.853	0.56 ± 0.75	1.43 ± 0.67
OGLE-TR-14	13.064	7.798	-0.18 ± 0.71	1.75 ± 0.65
OGLE-TR-15*	13.228	4.875	-1.87 ± 0.98	-0.12 ± 0.90
OGLE-TR-16	13.509	2.139	0.50 ± 1.92	14.16 ± 1.70
OGLE-TR-17	16.217	2.317	0.73 ± 0.94	1.01 ± 0.89
OGLE-TR-18	16.006	2.228	1.06 ± 0.81	4.30 ± 0.75
OGLE-TR-19*	16.352	5.282	-0.75 ± 1.12	0.21 ± 1.01
OGLE-TR-20*	15.407	4.284	0.11 ± 1.14	0.57 ± 1.04
OGLE-TR-21	15.585	6.893	0.01 ± 0.70	1.90 ± 0.65
OGLE-TR-22*	14.549	4.275	-4.28 ± 1.39	-0.29 ± 1.25
OGLE-TR-23*	16.396	3.287	-2.68 ± 1.11	-0.60 ± 1.04
OGLE-TR-24	14.843	5.282	2.05 ± 2.63	2.43 ± 2.20
OGLE-TR-25	15.274	2.218	0.23 ± 1.06	3.24 ± 0.98
OGLE-TR-26*	14.784	2.539	-0.17 ± 1.09	-0.23 ± 0.93
OGLE-TR-27	15.712	1.715	-0.31 ± 1.34	7.03 ± 1.25
OGLE-TR-28*	16.436	3.405	-1.30 ± 0.96	-1.72 ± 0.87
OGLE-TR-29*	15.646	2.716	3.34 ± 1.71	1.37 ± 1.55
OGLE-TR-30	14.923	2.365	0.29 ± 0.67	2.03 ± 0.60
OGLE-TR-31	14.332	1.883	-0.10 ± 0.86	3.88 ± 0.75

Table 1—Continued

Object name	$\langle I \rangle$	P_{orb}	a_{c1}	a_{c2}
OGLE-TR-32	14.849	1.343	1.02 ± 0.95	6.28 ± 0.87
OGLE-TR-33*	13.716	1.953	-0.83 ± 0.99	-2.15 ± 0.93
OGLE-TR-34*	15.997	8.581	-0.95 ± 0.42	0.17 ± 0.42
OGLE-TR-35*	13.264	1.260	3.96 ± 0.93	0.84 ± 0.85
OGLE-TR-36*	15.767	6.252	-0.69 ± 1.23	0.24 ± 1.08
OGLE-TR-37*	15.183	5.720	0.73 ± 0.98	-0.75 ± 0.90
OGLE-TR-38*	14.675	4.101	-1.06 ± 0.88	-0.19 ± 0.82
OGLE-TR-39	14.674	0.815	8.32 ± 1.12	5.37 ± 1.07
OGLE-TR-40*	14.947	3.431	0.46 ± 0.81	0.72 ± 0.72
OGLE-TR-41*	13.488	4.517	0.18 ± 0.62	-0.28 ± 0.56
OGLE-TR-42*	15.395	4.161	-0.05 ± 0.65	0.31 ± 0.60
OGLE-TR-47*	15.604	2.336	0.98 ± 0.78	0.46 ± 0.71
OGLE-TR-48*	14.771	7.226	-1.14 ± 0.99	0.20 ± 0.95
OGLE-TR-49*	16.181	2.690	0.70 ± 0.80	-1.21 ± 0.79
OGLE-TR-50*	15.923	2.249	-0.14 ± 0.86	0.39 ± 0.77
OGLE-TR-51*	16.716	1.748	0.76 ± 0.67	-0.22 ± 0.71
OGLE-TR-52	15.593	1.326	0.72 ± 1.24	3.71 ± 1.16
OGLE-TR-53	16.000	2.906	-0.04 ± 0.72	0.96 ± 0.68
OGLE-TR-54*	16.473	8.163	2.14 ± 1.20	-0.70 ± 1.08
OGLE-TR-55*	15.803	3.185	-0.60 ± 0.82	0.14 ± 0.75
OGLE-TR-56*	15.300	1.212	1.08 ± 0.46	-0.58 ± 0.43
OGLE-TR-57	15.695	1.675	0.73 ± 1.01	6.13 ± 0.95
OGLE-TR-58*	14.754	4.345	-2.51 ± 2.45	-3.07 ± 2.15
OGLE-TR-59	15.195	1.497	2.72 ± 0.81	1.89 ± 0.76
OGLE-TR-60	14.601	2.309	0.45 ± 0.42	1.40 ± 0.32
OGLE-TR-61	16.258	4.268	0.87 ± 1.18	8.60 ± 1.11
OGLE-TR-62	15.907	2.601	1.36 ± 0.67	3.09 ± 0.61
OGLE-TR-63*	15.751	1.067	0.08 ± 0.47	-0.26 ± 0.43
OGLE-TR-64*	16.169	2.717	0.38 ± 0.51	0.42 ± 0.49
OGLE-TR-65*	15.941	0.860	2.34 ± 0.55	-0.51 ± 0.51
OGLE-TR-66	15.180	3.514	-0.81 ± 0.56	1.11 ± 0.54

Table 1—Continued

Object name	$\langle I \rangle$	P_{orb}	a_{c1}	a_{c2}
OGLE-TR-67	16.399	5.280	1.39 ± 0.87	1.77 ± 0.74
OGLE-TR-68	16.793	1.289	0.62 ± 1.17	2.40 ± 1.12
OGLE-TR-69	16.550	2.337	1.90 ± 0.74	1.48 ± 0.69
OGLE-TR-70*	16.890	8.041	-0.83 ± 0.64	0.07 ± 0.61
OGLE-TR-71	16.379	4.188	-1.86 ± 0.50	0.97 ± 0.46
OGLE-TR-72*	16.440	6.854	1.49 ± 1.32	0.23 ± 1.16
OGLE-TR-73*	16.989	1.581	3.50 ± 0.97	-0.27 ± 0.86
OGLE-TR-74*	15.869	1.585	0.57 ± 1.11	0.56 ± 0.99
OGLE-TR-75	16.964	2.643	0.45 ± 0.69	2.46 ± 0.66
OGLE-TR-76	13.760	2.127	0.03 ± 0.66	0.90 ± 0.61
OGLE-TR-77*	16.122	5.455	0.26 ± 0.53	-0.07 ± 0.47
OGLE-TR-78	15.319	5.320	-0.36 ± 0.37	0.64 ± 0.32
OGLE-TR-79	15.277	1.325	0.02 ± 0.45	4.44 ± 0.44
OGLE-TR-80	16.501	1.807	2.16 ± 0.77	3.43 ± 0.71
OGLE-TR-81	15.413	3.216	-0.11 ± 0.96	2.38 ± 0.86
OGLE-TR-82*	16.304	0.764	0.23 ± 0.84	0.59 ± 0.69
OGLE-TR-83	14.865	1.599	1.71 ± 0.71	5.38 ± 0.66
OGLE-TR-84	16.692	3.113	-0.16 ± 0.68	1.28 ± 0.64
OGLE-TR-85	15.452	2.115	-0.26 ± 0.53	1.17 ± 0.41
OGLE-TR-86	16.319	2.777	1.70 ± 0.89	0.95 ± 0.80
OGLE-TR-87*	16.321	6.607	-0.43 ± 0.61	-0.20 ± 0.56
OGLE-TR-88	14.578	1.250	1.13 ± 0.67	3.23 ± 0.62
OGLE-TR-89*	15.782	2.290	0.45 ± 0.40	0.03 ± 0.36
OGLE-TR-90	16.441	1.042	-0.65 ± 0.60	1.51 ± 0.56
OGLE-TR-91	15.231	1.579	0.42 ± 1.20	6.55 ± 1.16
OGLE-TR-92	16.496	0.978	-0.21 ± 0.56	3.31 ± 0.50
OGLE-TR-93	15.198	2.207	0.28 ± 0.62	3.13 ± 0.57
OGLE-TR-94	14.319	3.092	0.44 ± 0.54	1.99 ± 0.48
OGLE-TR-95	16.366	1.394	-2.49 ± 0.89	2.58 ± 0.83
OGLE-TR-96*	14.900	3.208	-0.00 ± 0.56	-0.04 ± 0.47
OGLE-TR-97	15.512	0.568	0.79 ± 0.67	1.08 ± 0.63

Table 1—Continued

Object name	$\langle I \rangle$	P_{orb}	a_{c1}	a_{c2}
OGLE-TR-98*	16.639	6.398	0.30 ± 0.47	-0.16 ± 0.45
OGLE-TR-99	16.469	1.103	1.21 ± 0.65	3.11 ± 0.57
OGLE-TR-100	14.879	0.827	0.95 ± 0.85	2.30 ± 0.81
OGLE-TR-101	16.689	2.362	-0.08 ± 0.78	2.72 ± 0.70
OGLE-TR-102	13.841	3.098	-0.67 ± 0.33	0.40 ± 0.30
OGLE-TR-103*	16.694	8.217	-0.41 ± 0.42	-0.61 ± 0.42
OGLE-TR-104*	17.099	6.068	-0.27 ± 0.68	-0.12 ± 0.64
OGLE-TR-105*	16.160	3.058	0.98 ± 1.00	-0.59 ± 0.85
OGLE-TR-106	16.529	2.536	1.32 ± 0.89	1.01 ± 0.77
OGLE-TR-107*	16.664	3.190	-0.91 ± 0.84	0.11 ± 0.74
OGLE-TR-108	17.282	4.186	0.19 ± 0.94	1.89 ± 0.88
OGLE-TR-109	14.990	0.589	0.77 ± 0.35	0.60 ± 0.33
OGLE-TR-110	16.149	2.849	0.51 ± 0.51	0.60 ± 0.47
OGLE-TR-111*	15.550	4.016	0.02 ± 0.45	-0.26 ± 0.41
OGLE-TR-112	13.641	3.879	0.65 ± 0.43	1.23 ± 0.37
OGLE-TR-113*	14.422	1.433	-0.73 ± 0.45	-0.70 ± 0.39
OGLE-TR-114*	15.763	1.712	0.30 ± 0.86	-0.95 ± 0.79
OGLE-TR-115*	16.658	8.347	0.58 ± 0.60	0.12 ± 0.57
OGLE-TR-116*	14.899	6.064	-0.34 ± 1.00	0.31 ± 0.77
OGLE-TR-117	16.710	5.023	-0.19 ± 0.67	0.72 ± 0.62
OGLE-TR-118	17.073	1.861	0.78 ± 0.63	1.19 ± 0.59
OGLE-TR-119	14.291	5.283	-0.11 ± 0.92	0.87 ± 0.74
OGLE-TR-120*	16.229	9.166	-0.46 ± 0.63	0.34 ± 0.57
OGLE-TR-121	15.861	3.232	-0.21 ± 0.71	1.84 ± 0.60

Note. — Objects marked with an asterisk (*) are those for which $a_{c2} < b_2$, i.e. stars which do not exhibit ellipsoidal variability and are thus planetary system candidates.

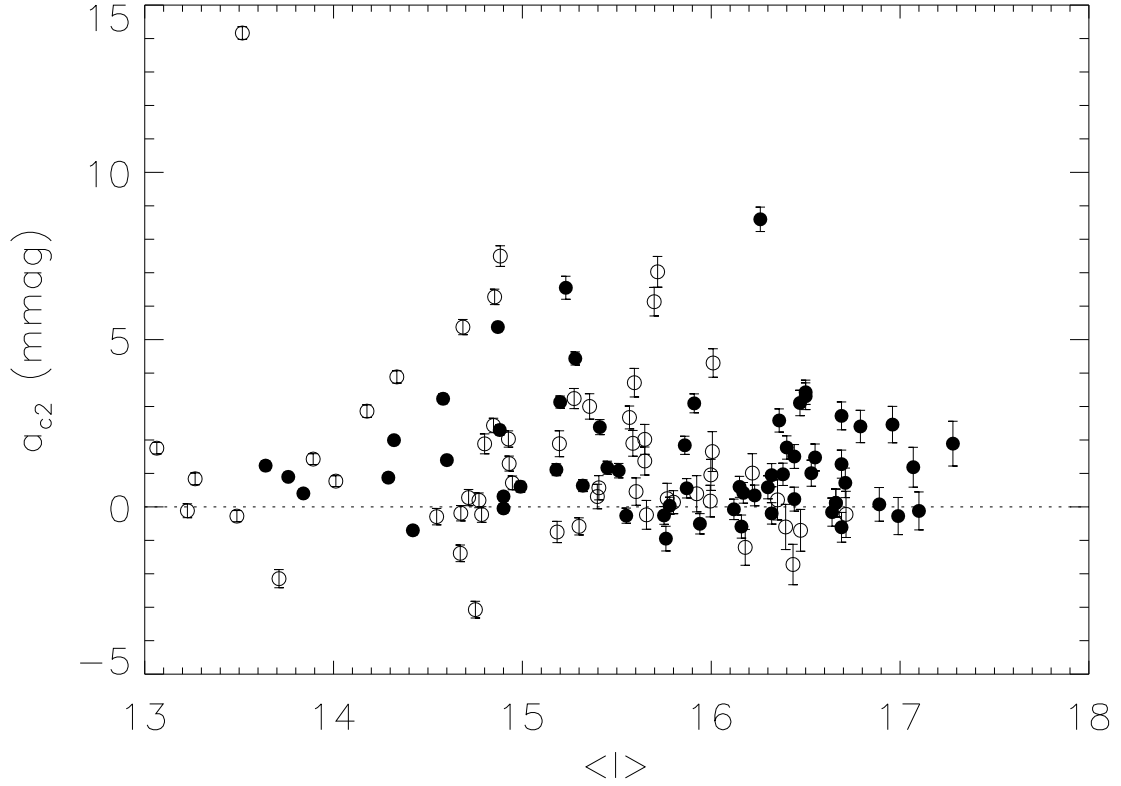


Fig. 1.— The values of the parameter corresponding to ellipsoidal light variations are shown as a function of average stellar magnitude $\langle I \rangle$. Open and filled symbols refer to the data sets OGLE TR-1 to TR-59 and TR-60 to TR-121, respectively. Formal errors obtained with the least squares fit are also shown. Note a number of stars with negative, i.e. not physical, values of a_{c2} , which are many formal standard deviations below zero. This indicates that the errors are not realistic.

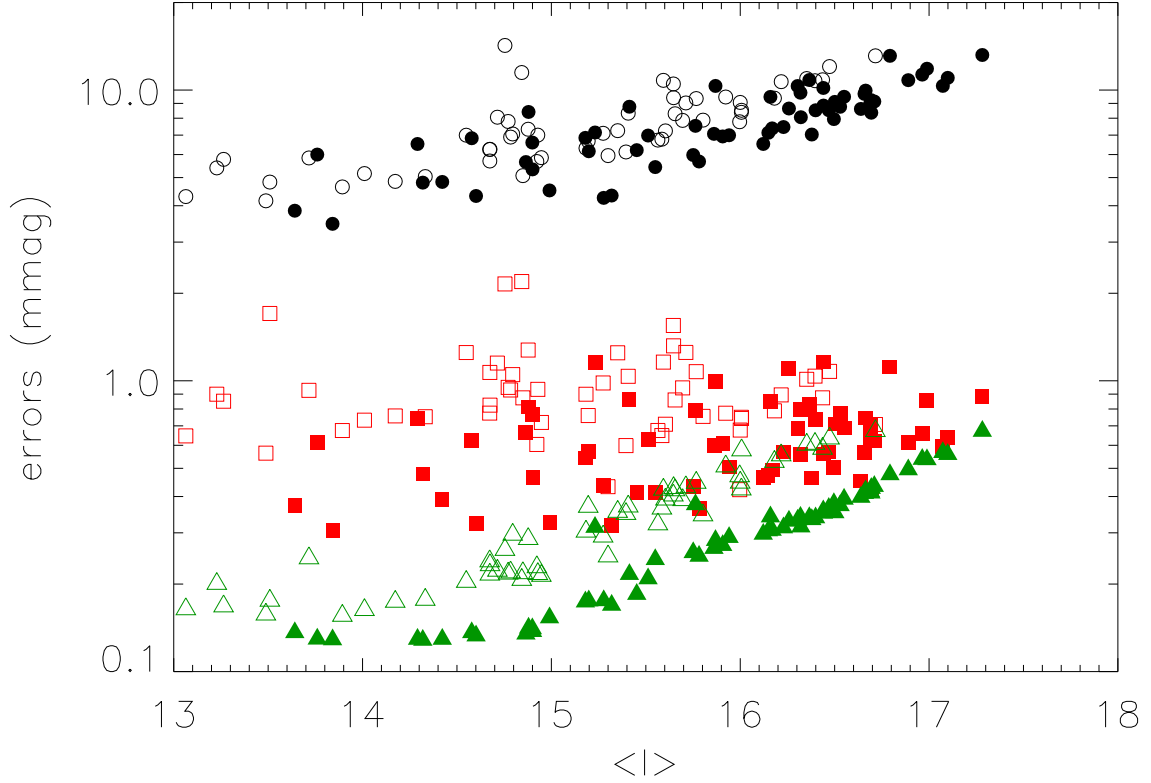


Fig. 2.— Photometric errors are shown as a function of $\langle I \rangle$ magnitude. Black circles refer to the errors of individual data points, defined as an rms deviation from a 5 parameter fit to the light curves outside of the transits (cf. eq. 1). The two outliers near $\langle I \rangle \approx 14.8$, stars TR-24 and TR-58, have a long term variability at the level of 0.015 mag. Green triangles are the average of the formal errors of the 5 parameter fit obtained with the least squares solution of eq. (1). Red squares are the errors of the a_{c2} term determined with our spectral analysis - note they are considerably larger than the formal errors, as the photometric data have a strong time correlation. Open and filled symbols refer to the OGLE TR-1 to TR-59 and TR-60 to TR-121 data sets, respectively.

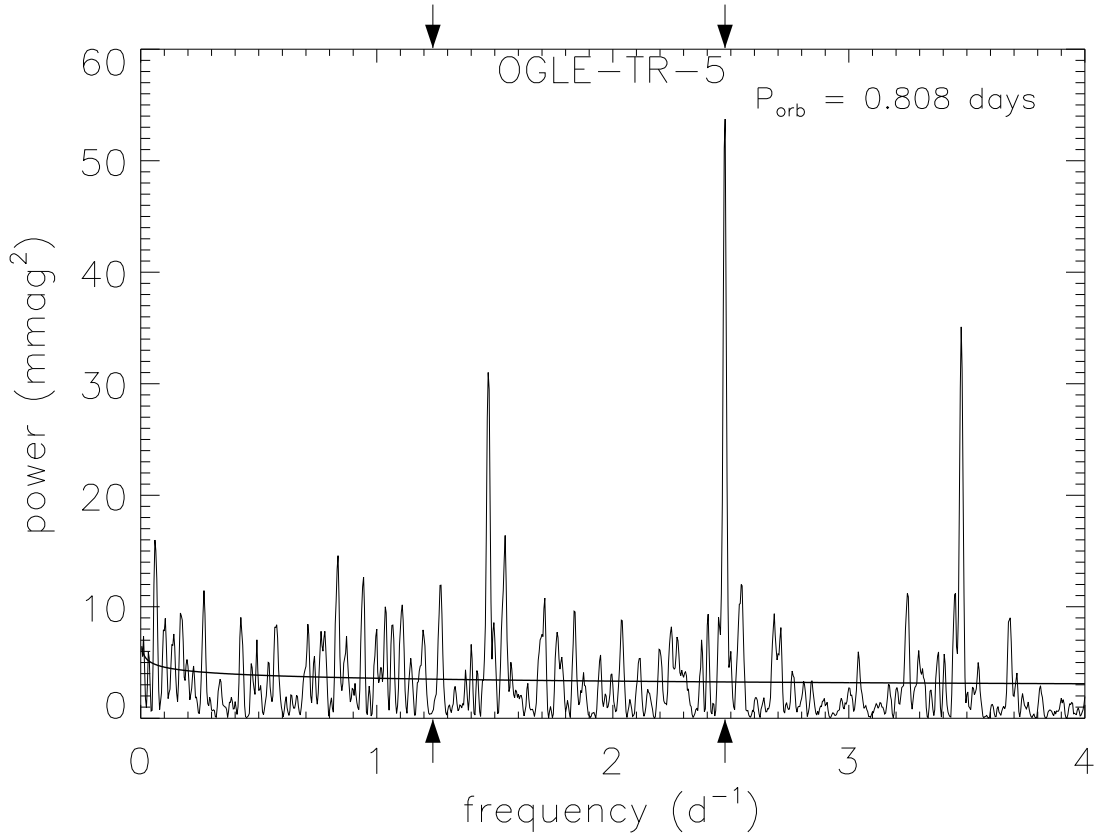


Fig. 3.— The power spectrum is shown for OGLE-TR-5. The thick solid line is the least squares power law fit to the spectrum. The two arrows correspond to the orbital frequency $1/P_{\text{orb}} = 1.237 \text{ d}^{-1}$, and the frequency of expected ellipsoidal variability $2/P_{\text{orb}} = 2.475 \text{ d}^{-1}$. Notice a very strong peak at the ‘ellipsoidal’ frequency, and the two aliases at 1.475 d^{-1} and at 3.475 d^{-1} .

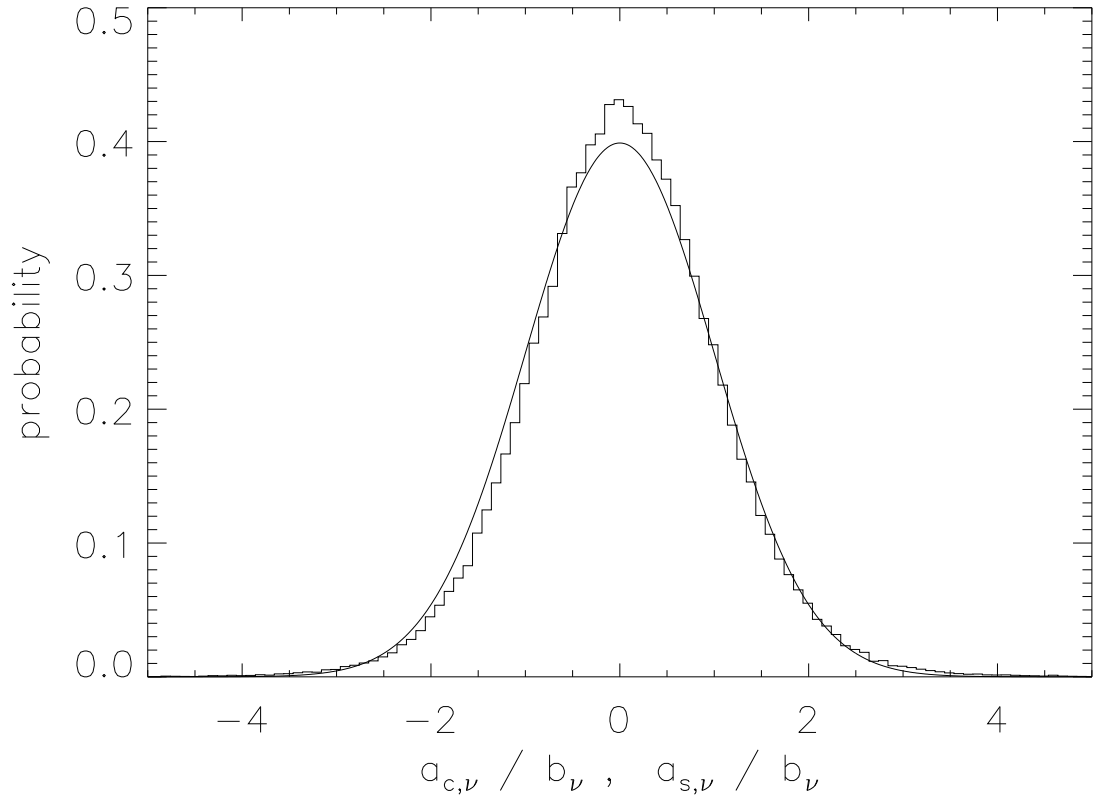


Fig. 4.— The distribution of normalized amplitudes of sine and cosine terms for all sampled frequencies and for all transit candidates except OGLE-TR-24 and TR-58. For comparison a Gaussian distribution with unit variance is also shown.

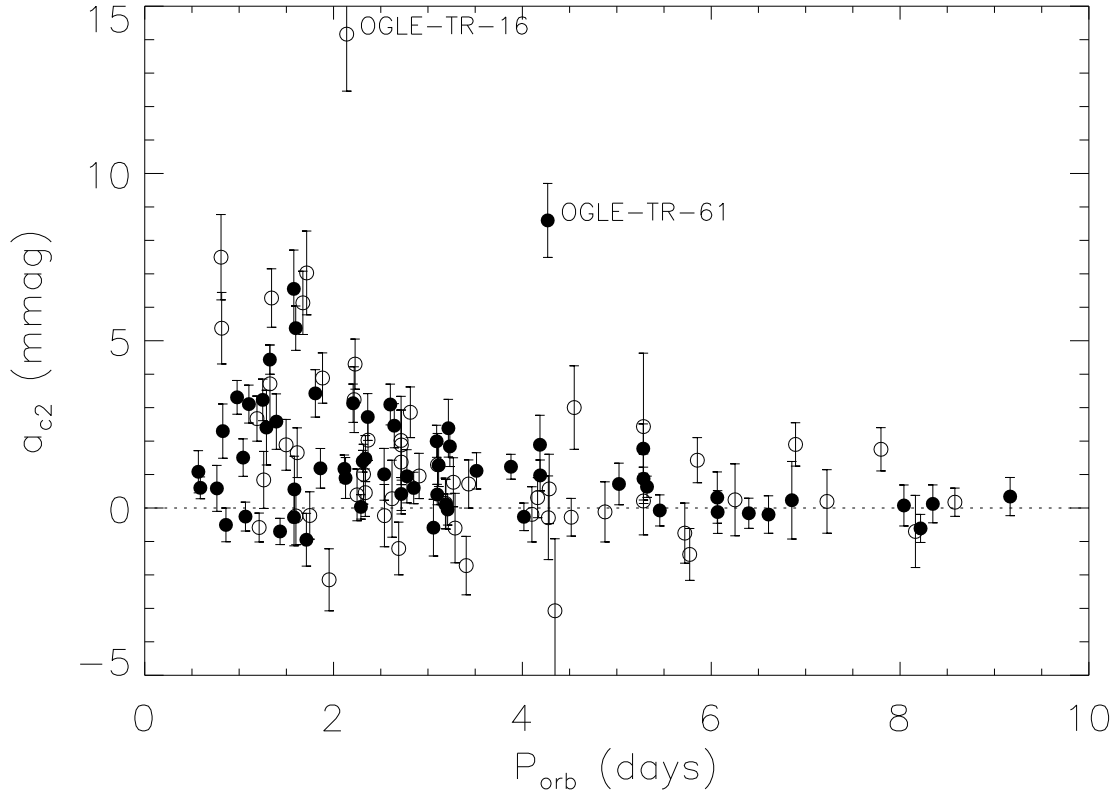


Fig. 5.— The values of the parameter a_{c2} , corresponding to ellipsoidal light variations, are shown as a function of orbital period, P_{orb} . Open and filled symbols refer to the stars OGLE TR-1 to TR-59, and TR-60 to TR-121, respectively. The errors are based on the limited spectral analysis presented in this paper. None of the negative values are significant. Up to $\sim 50\%$ of all stars may have significant ellipsoidal variability, indicating a massive, not planetary, companion.

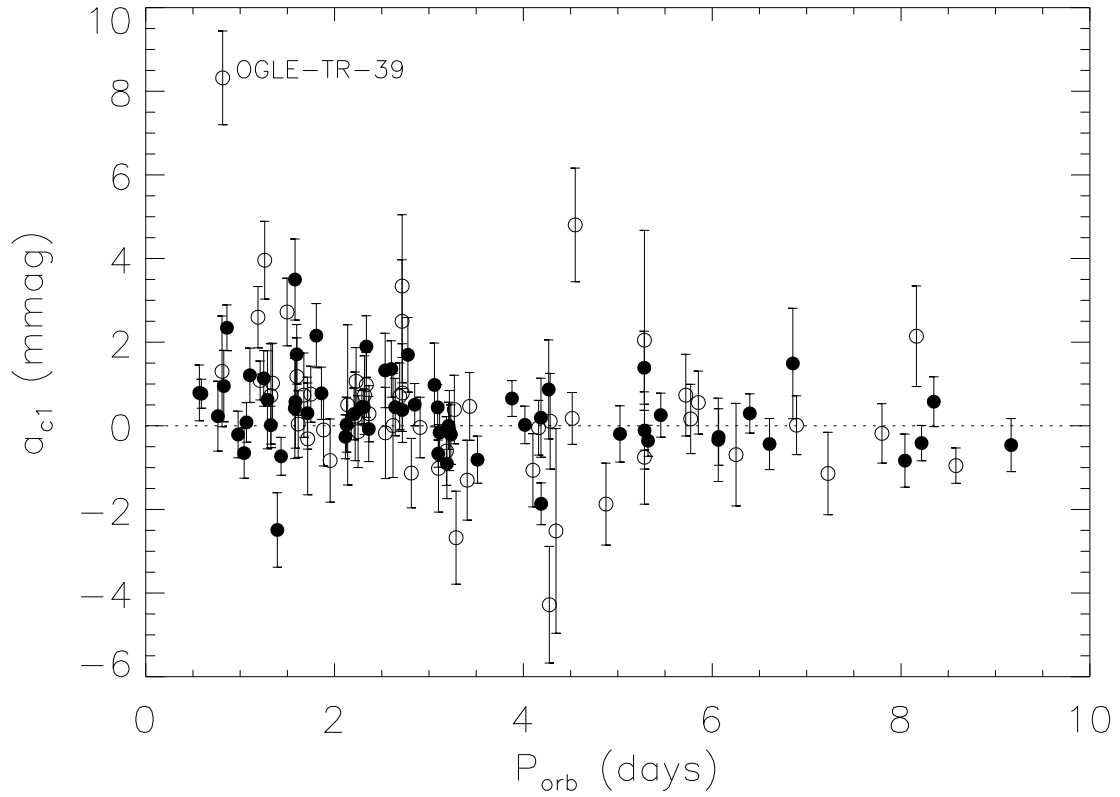


Fig. 6.— The same as Fig. 5, but for the a_{c1} parameter, which is indicative of possible ‘heating’ (reflection) effects of the companion’s hemisphere facing the primary. Only OGLE-TR-39 shows the effect strongly, but there may be several other stars for which the effect is real.

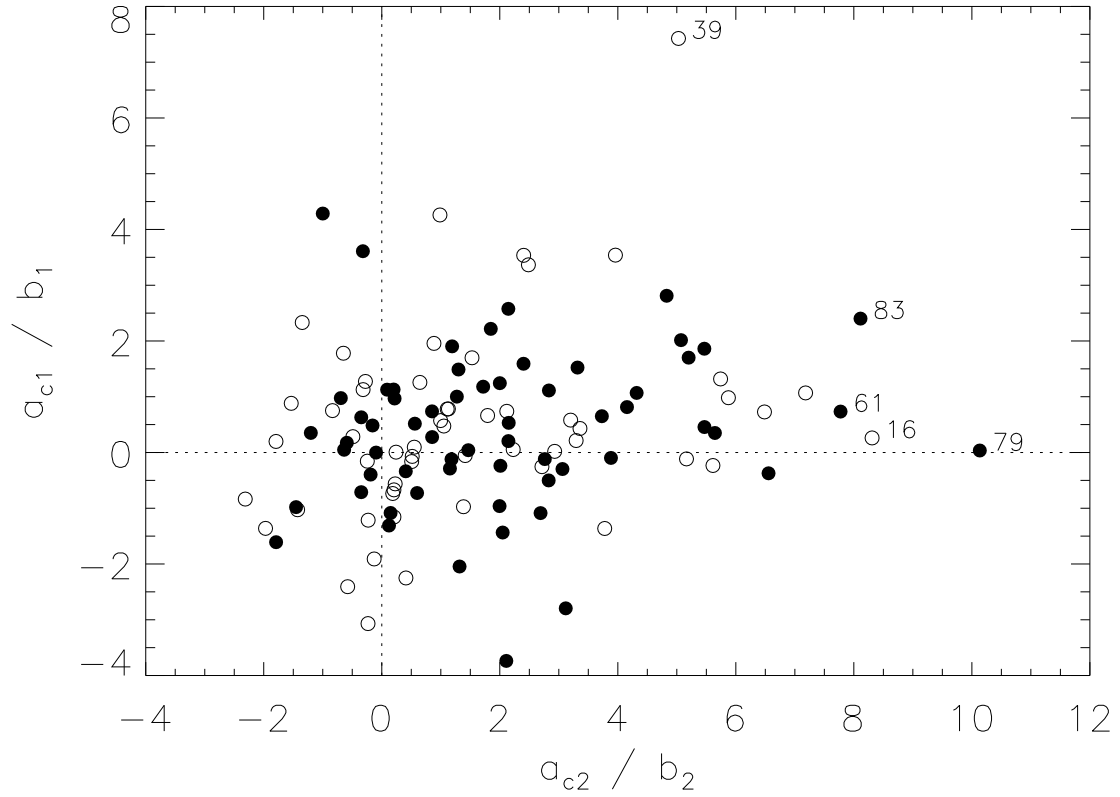


Fig. 7.— A relation between the ellipsoidal variability parameter a_{c2} , and the heating variability parameter a_{c1} (cf. eq. 1), both normalized by their errors. The stars with the strongest effects are labeled with their OGLE names. The negative values of either parameter are consistent with them being due to errors.

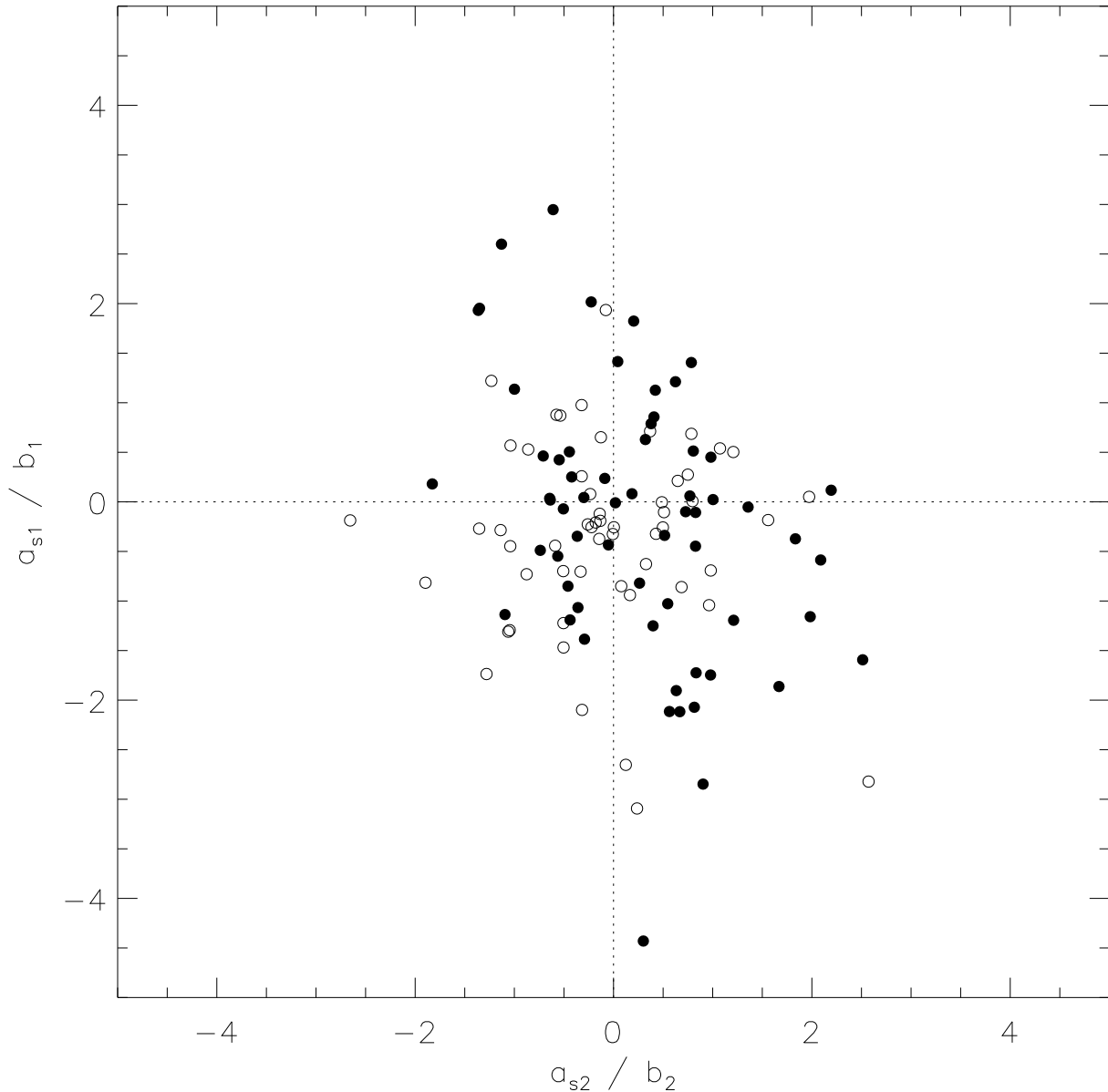


Fig. 8.— A relation between the coefficients of the sine terms in eq. (1), normalized by their errors. The ratio of the number of stars with the values of either coefficient being within one σ of zero, to the number outside of one σ is approximately 3/1, not very different from the ratio 2/1 expected if their true values were zero and their distributions were Gaussian. We conclude that our error estimate is reasonable, and we have no coefficients a_{s1} or a_{s2} that are measurably non-zero, with the possible exception of OGLE-TR-68, the filled circle with $a_{s1}/b_1 = -4.4$. Visual inspection of its light curve clearly shows that the system is approximately 15 mmag brighter at phase 0.25 than it is at phase 0.75.